 doi:10.20944/preprints202105.0466.v1

Articles

Dye-sensitized solar cell for building-integrated photovoltaic (BIPV) applications

Marek Szindler [1*], Magdalena Szindler [2], Aleksandra Drygała [2], Krzysztof Lukaszkowicz [2] and Paulina Kaim [2], Rafał Pietruszka[3]

1 Scientific and Didactic Laboratory of Nanotechnology and Material Technologies, Faculty of Mechanical Engineering, Silesian University of Technology, Towarowa 7 Str., 44-100 Gliwice, Poland
2 Department of Engineering Materials and Biomaterials, Silesian University of Technology, Konarskiego 18a Str., 44-100 Gliwice, Poland
3 Institute of Physics, Polish Academy of Sciences, Warsaw, Poland
* Correspondence: marek.szindler@polsl.pl

Abstract: One of the important research directions in the field of photovoltaics is integration with construction. The integration of solar cell systems with a building can reduce installation costs and help optimize the used space. One of the interesting types of cells is dye-sensitized solar cells. In addition to their interesting properties, they also have aesthetic value. In the classic arrangement, they are constructed using glass with a transparent conductive layer (TCL). This article describes replacing a classic glass counter electrode with an electrode based on a ceramic tile and nickel foil. This solution makes it possible to expand their construction applications. The advantage of this solution is full integration with construction while simultaneously generating electricity. A dye-sensitized solar cell was built layer-by-layer on ceramic tile and nickel foil. An atomization method was used to deposit fluorine-doped tin oxide, and then a screen printing method was used to deposit a platinum layer. The electrical parameters of the manufactured DSSCs with and without a counter electrode tile were characterized by measuring their current-voltage characteristics under standard AM 1.5 radiation. A dye-sensitized solar cell integrated with ceramic tiles and nickel foil was produced and displayed an efficiency of over 4%.

Keywords: Renewable energy, Nanotechnology, Building-integrated photovoltaics (BIV), Thin films, Dye-sensitized solar cells

1. Introduction

Photovoltaics is a field covering the issues of obtaining electricity from sunlight, as well as its processing and storage [1]. The first efficient (6%) crystalline silicon solar cells were made by Chapin, Fuller, and Pearson of Bell Laboratories in 1953 by diffusing boron into n-type silicon [2]. Five years later, Maldenkorn and colleagues at the United States Army Electronics Research and Development Laboratories in Belmar, NJ developed n-p solar cells. In the summer of 1960, RCA Laboratories showed that these solar cells were much more resistant to cosmic rays than p-n cells, which led to extremely intense research and development into silicon solar cells for use as energy sources in spacecraft [1-2]. During the 1970s energy crisis, the idea of also using solar cells for terrestrial purposes began, which made work related to the improvement of solar cell technology one of the most attractive research directions [3]. In the 1970s, PV modules were initially installed on buildings where there was no access to traditional electricity [4]. It was not until the 1980s that the first modules mounted on the roofs of single-family houses were presented [3-4]. The concept of integrated photovoltaics in construction is based on the direct use of PV modules in buildings as an alternative to traditional building structures such as roofing and facade systems. There are several products in the field of integrated photovoltaics. One group of materials is thin-film solar cells in the form of foil, which was described by Jelle B.P. et al. [5]. The above solution has a low deadweight, but it is not resistant to external weather conditions. This solution can be used as a facade element. Another

Preprints (www.preprints.org) | NOT PEER-REVIEWED | Posted: 20 May 2021 doi:10.20944/preprints202105.0466.v1

solution is solar cells mounted on tiles or partially replacing tiles based on silicon photovoltaic cells as described Yen-Chieh Huang et al. [6]. There are also ready-made photovoltaic modules for use on roofs, which differ from the classic use of elements that protect against weather conditions. They are most often fitted to ready-made roof solutions as described in M. Debbarma et al. [7]. Of the four generations of solar cells, one of the most interesting types is dye-sensitized solar cells, which use processes similar to those occurring in nature to convert solar energy into electricity (the difference is that their donor-acceptor systems transform light energy into electricity, and not into chemical energy as in photosynthesis) [8-10]. The working principle of such solar cells is slightly different from typical organic solar cells. A dye-sensitized solar cell consists of two glasses with transparent conductive oxide (TCO) layers as electrodes [11-14]. On the photoelectrode surface, there is an n-type semiconductor layer with a wide energy gap made of a two-component metal oxide such as TiO_2, ZnO, etc. The metal oxide is a poor photon absorber, but association with organic dye molecules increases its conductivity. The dye is also a photosensitizer that absorbs photons of solar radiation in the range between 400 – 700 nm. The most commonly used dyes are organometallic compounds, including the compounds of ruthenium, osmium, and copper [13-15]. The electrolyte that fills the surface between the semiconductor layer and the anode is usually a solution containing the I/I^{3-} redox system. The electrolyte's task is to transfer electrons to the oxidized dye so that it returns to its basic state. The construction of a dye-sensitized solar cell closes the counter electrode (Figure 1). The task of the counter electrode is to collect electrons flowing from an external current to catalyze the reduction of ions in the electrolyte. Platinum is the most commonly used material for the counter electrode [16-20].

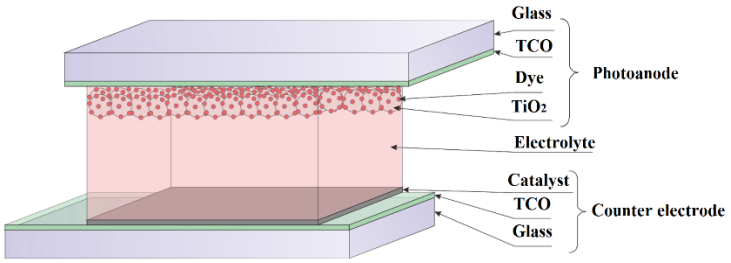

Figure 1. The scheme of a classical dye-sensitized solar cell.

Replacing glass in a DSSC with other materials such as light and flexible plastics films, metals, steel, or paper may decrease costs because the glass substrate constitutes 15–20% of the price of a photovoltaic cell. Additionally, the price of PET/ITO substrates has increased by 250% in the last 10 years, which makes it an expensive material to produce solar cells [14]. This article presents the results of research on the manufacture of innovative dye-sensitized solar cells on the surface of low-cost ceramic tile and nickel foil.

2. Material descriptions and research methodology

The developed solar cells consist of three elements: a photoanode, a liquid electrolyte, and a counter electrode. In the first stage, in order to produce a counter electrode, a layer of transparent conductive oxide in the form of fluorine-doped tin oxide (FTO) was deposited by atomization on ceramic tile and nickel foil. This method is based on the deposition of a sol on the surface of a substrate using a bottle with an atomizer. The application of this method allows the temperature of the substrate to be controlled in a wider range than conventional spraying deposition methods. Moreover, deposition by atomization does not require an additional carrier gas for spraying. In the first stage, in order to produce a counter electrode, a layer of transparent conductive oxide in the form of fluorine-doped tin oxide (FTO) was deposited by an atomization method. Dibutyltin diacetate (DBTDA) was dissolved in ethanol. NH_4F was dissolved in water. These two solutions were mixed and agitated ultrasonically for 30 min. This mixture was sprayed onto a heated ceramic tile and nickel foil (surface

Preprints (www.preprints.org) | NOT PEER-REVIEWED | Posted: 20 May 2021 doi:10.20944/preprints202105.0466.v1

temperature = 100 °C) by the bottle with an atomizer. Then, nanocolloidal platinum paste (Sigma Aldrich) was used as a catalytic counter electrode. Platinum paste was applied to the FTO ceramic tile using a screen-printing method. The layer thickness was about 0.5 μm. In this article, an MS300FRO screen-printing machine was used. After printing, the wet film was dried at 125 °C for 10 minutes, and two more layers were applied. After that, three layers of platinum paste were sintered in an oven. The oven was heated from room temperature to 500 °C with a heating rate of 15 °C/min and maintained at 500 °C for 30 minutes. In the next stage, in order to produce a photoanode, on the commercially-available FTO glass plate (in case of a ceramic tile) and PET/ITO (in the case of nickel foil), a titanium oxide nanolayer was deposited by an atomic layer method. Then, a layer of porous nanocrystalline titanium oxide was applied by a screen printing method (18 NR-T, Greatcell Solar). The dye (N719, Sigma Aldrich) was then applied by dipping the glass plates with deposited layers in an ethyl alcohol dye solution to obtain the final form of the photoanode. In the last stage, in order to obtain integrated dye-sensitized solar cells, the counter electrode and photoanode were joined together with the layers directed inwards, and a liquid electrolyte (EL-HSE, Sigma Aldrich) containing an I^-/I^{3-} redox couple was placed between them by spotting. The scheme of the produced DSSCs is shown in Figure 2.

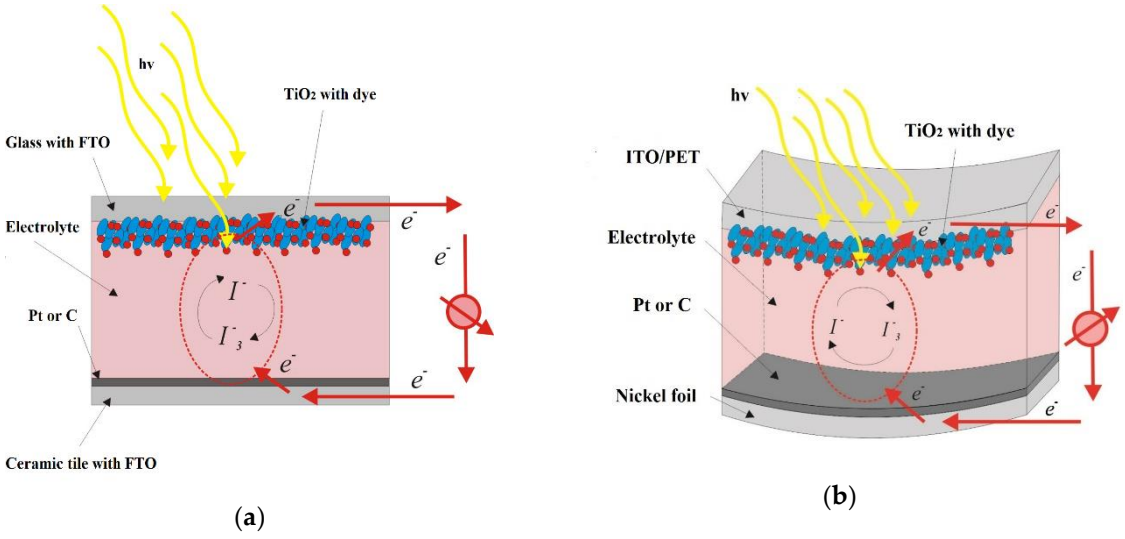

Figure 2. The scheme of a prepared building integrated dye sensitized solar cells with ceramic tile (a) and nickel foil (b) counter electrode

Scanning electron microscope (SEM) images were taken with a Zeiss Supra 35. The accelerating voltage was 5 kV. To obtain images of the surface topography, the secondary electron detector (by the in-lens detector) was used. Qualitative studies of chemical composition were also performed using energy-dispersive spectrometry (EDS). Electrical parameters were obtained from Hall Effect measurements. An RH2035 Phys-Tech GmbH system operating at a magnetic field of $B = 0.426$ T was used. The measurements were carried out at room temperature in the Van der Pauw mode. Electrical contacts (Al) were sputtered by a PVD 75 Kurt J. Lesker system. Further structural testing of deposited thin films was performed using an inVia Reflex Raman spectrometer equipped with an Arion laser with a 514.5 nm length for a spectral range of 150–3200 cm^{-1}. X-ray diffraction studies were carried out on an X'Pert Pro MPD diffractometer by PANalytical, using filtered (Fe filter) radiation from an X-ray tube with a cobalt anode (Co $\lambda = 1.7909$ Å), supplied with 40 kV voltage, with a filament current of 30 mA. A PIXcell 3D state detector was applied on the axis of the diffracted beam. X-ray diffraction measurements were made in the Bragg-Brentano geometry in the angle range 20–80° [2θ] with a 0.05° step and a counting time of 60 s per step. The obtained diffractograms were analyzed using X'Pert High Score Plus software, together with the dedicated structural database PAN-ICSD. The results were processed by the WiRE3.1 program. The value of electric charge transfer from the counter electrode to the electrolyte was investigated using electrochemical impedance

Preprints (www.preprints.org) | NOT PEER-REVIEWED | Posted: 20 May 2021 doi:10.20944/preprints202105.0466.v1

spectroscopy (EIS). The electrochemical measurements were made using a potentiostat-galvanostat coupled with an impedance meter (ATLAS 0531 EU&IA). The impedance spectra were recorded in the range of 0.05–105 Hz, for the alternating-current excitation amplitude V_{ac} of 10 mV, at open-circuit voltage. A platinum electrode was used as the reference electrode. The EIS measurements were made in an electrolyte solution consisting of LiI (0.5 mol L^{-1}), I_2 (0.05 mol L^{-1}), and 4-*tert*-butylpyridine (0.6 mol L^{-1}) in acetonitrile. For the interpretation of the obtained spectra, the electric Randles equivalent system shown in Figure 3 was used, which contains the resistive element *Rs*, corresponding to the resistance of the solution (which does not depend on the catalytic layers, but on the type of electrolyte used), which is set up with two series-connected systems: resistance (R_{ct}), Warburg impedance (*W*), and a constant-phase element (*Q*). R_{ct} characterizes the charge transfer resistance of the counter electrode and the charge recombination resistance of the photoanode, while the Warburg impedance (*W*) relates to the ion diffusion resistance of the electrolyte. Element *Q* is the double-layer capacitance, which was used due to spatial inhomogeneities at the photoanode/electrolyte interface and surface imperfections such as layer porosity and surface roughness.

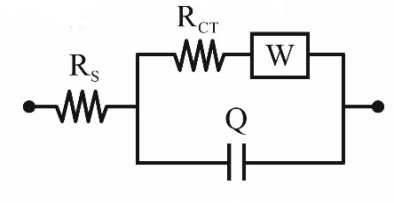

Figure 3. The Randles electrical equivalent system.

The electrical parameters of the manufactured DSSCs were characterized by measurements of current-voltage (I-V) characteristics using a PV Test Solutions Tadeusz Zdanowicz Solar Cell I-V Tracer System and a Keithley 2400 source meter under standard AM 1.5 radiation.

3. Results and Discussion

SEM images were taken with a Zeiss Supra 35 using an accelerating voltage of 5 kV (Figure 4). To obtain images of the surface topography, the secondary electron (in-lens) detector was used. In both cases, an even, continuous layer with no visible defects was obtained. In turn, the application of substrate heating initiated the crystallization of the FTO layer. The grain size did not exceed 100 nm.

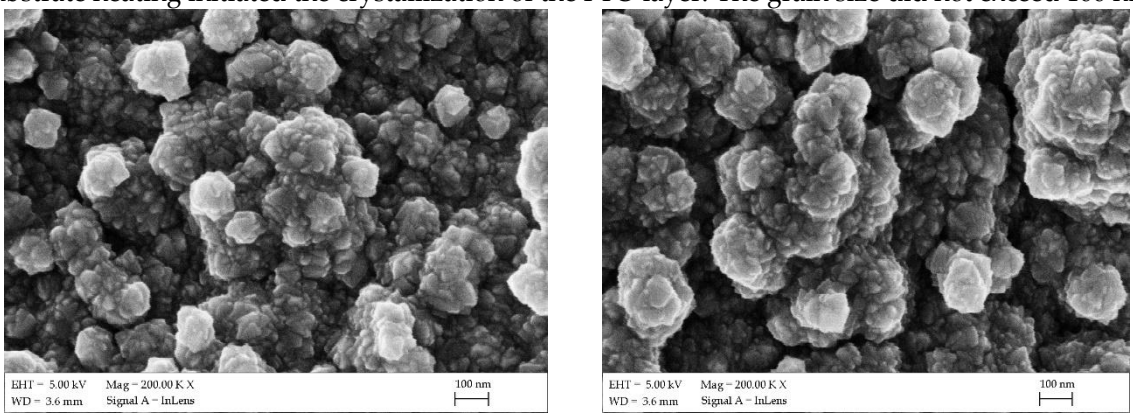

(**a**) (**b**)

Figure 4. SEM surface topography images of the FTO sprayed thin film on the ceramic tile (a) and nickel foil (b).

Qualitative studies of the chemical composition were also performed using energy-dispersive spectrometry (EDS), which recorded reflections characteristic of tin, fluorine, and oxygen from the layer (Figure 5). For tin, lines at 3.444 eV (spectrum line Lα1) and at 3.663 eV (spectrum line Lβ1)

Preprints (www.preprints.org) | NOT PEER-REVIEWED | Posted: 20 May 2021 doi:10.20944/preprints202105.0466.v1

were registered. Oxygen appeared at 0.525 eV (spectrum line Kα1), and a low fluoride content was also recorded at 0.677 eV (spectrum line Kα1).

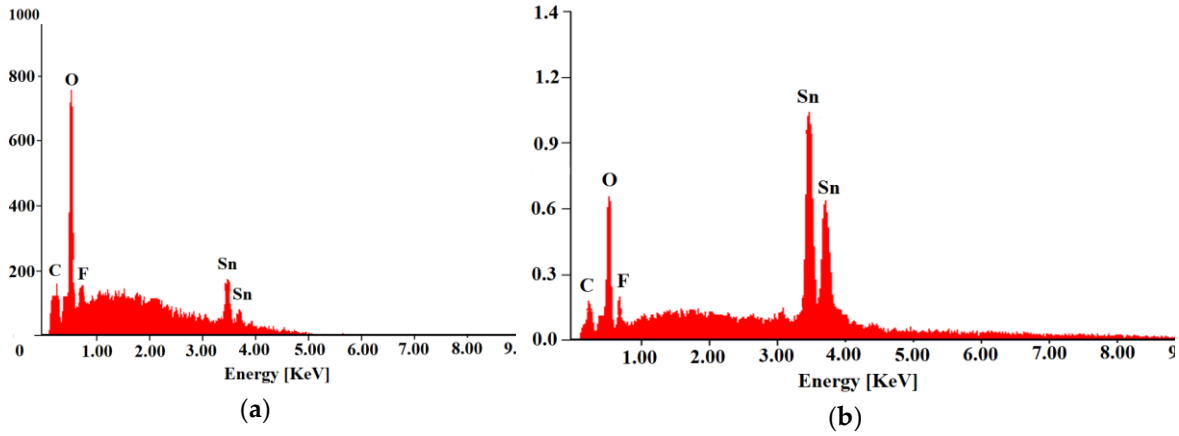

Figure 5 EDS spectrum of the FTO sprayed thin film on the ceramic tile (a) and nickel foil (b).

Table 1 presents the electrical parameters of the FTO samples deposited on the ceramic tile and nickel foil. The influence of the applied substrate temperature on the electrical properties was observed. An increase in the carrier concentration and mobility was recorded. As a result, the resistivity of the deposited layers decreased. The layer deposited on the heated substrate displayed a resistivity of 5.76 × 10^{-3} Ω cm, a carrier mobility of 19 cm^2/V s, and a carrier concentration of 4 × 10^{19} cm^{-3}.

Table 1. Electrical parameters of the investigated FTO layers: resistivity (ρ), carrier concentration (n), and carrier mobility (μ).

FTO samples	***ρ [Ω·cm]***	***n [cm^{-3}]***	***μ [cm^2/V·s]***
Nickel foil (non heated)	1.23 x 10^{-4}	2.68 x 10^{21}	24.20
Nickel foil (Heated=100°C)	5.69 x 10^{-5}	4.52 x 10^{21}	24.30
Ceramic tile (non heated)	1.26 x 10^{-4}	2.71 x 10^{21}	24.10
Ceramic tile (Heated=100°C)	5.76 x 10^{-5}	4.54 x 10^{21}	24.30

Raman spectrometry is a helpful tool for evaluating the quality of a prepared layer. Raman spectra make it possible to identify particles and study their structure. The Raman spectra of the FTO layer deposited on different surfaces (ceramic tile and nickel foil) were recorded (Figure 6). For the deposited FTO layer, vibration bands for SnO and SnO_2 molecules were recorded at 115, 244, 474, 494, 561, 633, and 772 cm^{-1}. According to group theory, rutile SnO_2 belongs to the D4h point group. The Γ point can be presented at: Γ = A1g + A2g + A2u + B1g + B2g +2B1u + Eg + 3Eu. At a wavenumber of 474 cm^{-1}, vibrations of oxygen were recorded (*Eg*). The bands at Raman shifts of 633 and 772 cm^{-1} correspond to the A1g and B2g vibration modes, respectively. The A1g and B2g modes are related to the vibration mode of the expansion and contraction of SnO bonds.

Preprints (www.preprints.org) | NOT PEER-REVIEWED | Posted: 20 May 2021 doi:10.20944/preprints202105.0466.v1

Products such as clay, quartz, and dyes are used to make ceramic tiles. Clay is mainly composed of silicon oxides (SiO_2 approx. 50%), rare earth oxides (R_2O_3 approx. 25%), aluminum oxides (Al_2O_3 approx. 15%), and oxides of iron, titanium, magnesium, calcium, and potassium (approx. 10%). Therefore, ceramic tile is a product that consists of many different molecules, as shown in the Raman spectrum. The bands derived from the vibrations of SiO_2 were recorded at 321, 335, 354, 393, and 454 cm^{-1} wavelengths. Rare earth molecules, depending on their composition, produce bands in the range of 95–660 cm^{-1}. The vibrations of aluminum oxide molecules produce bands at 360, 400, 460, 610, and 620 cm^{-1}. Bands originating from the vibrations of iron oxide molecules were recorded at 220, 300, 410, 500, and 620 cm^{-1}. At 150, 400, 520, and 645 cm^{-1}, bands from vibrations of titanium dioxide molecules were also recorded. The vibrations of the MgO molecule produced bands at 420, 476, and 594 cm^{-1}. Small bands from the vibrations of the CaO molecule at 464, 522, and 553 cm^{-1} were also recorded. The typical signals for the NiO_x layer on the Ni metal surface were recorded—the bands due to the stretching mode of the NiO molecule were recorded at 540 and 800 cm^{-1}.

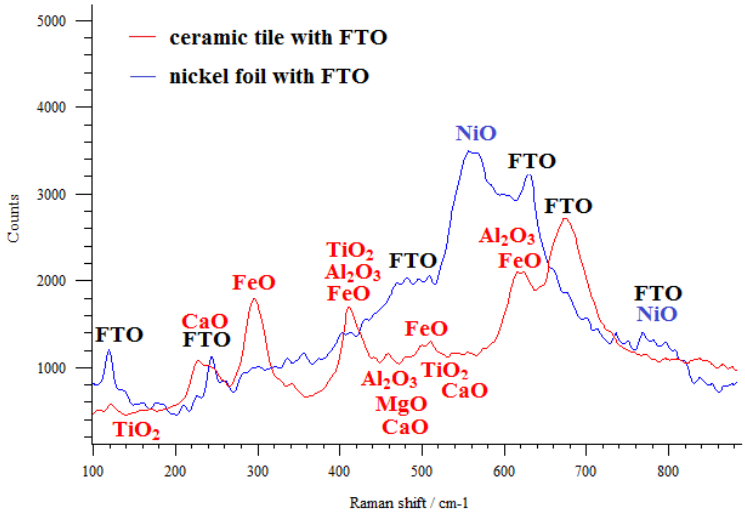

Figure 6 Raman spectra of the FTO sprayed thin film on the ceramic tile and nickel foil.

Platinum paste was applied on an FTO ceramic tile using a screen-printing method. The layer thickness was about 0.5 µm. In this article, a screen-printing machine (MS300FRO) was used. After printing, the wet film was dried at 125 °C for 10 minutes, and two more layers were applied. After that, three layers of platinum paste were sintered in an oven. The oven was heated from room temperature to 500 °C with a heating rate of 15 °C/min and maintained at 500 °C for 30 minutes. Platinum tends to increase as the so-called "islands" (Figure 7). The figures document the structure of the FTO with deposited platinum islands; however, a greater packing density was recorded on the FTO deposited on the ceramic tile substrate. To confirm that the observed thin films are platinum, qualitative chemical composition was studied using EDS spectra, and the reflections typical for platinum at 2.127 keV (spectrum line Mβ1) were registered (Figure 8).

To analyze the diffractogram, JCPDS files were used, according to which the appropriate Miller indices were assigned. Platinum thin films were characterized by a constant angle of incidence identifying characteristic peaks of platinum and tin oxide. The crystal structure for platinum was identified as face-centered cubic based on card No. 98-018-3075 (Figure 9).

Preprints (www.preprints.org) | NOT PEER-REVIEWED | Posted: 20 May 2021 doi:10.20944/preprints202105.0466.v1

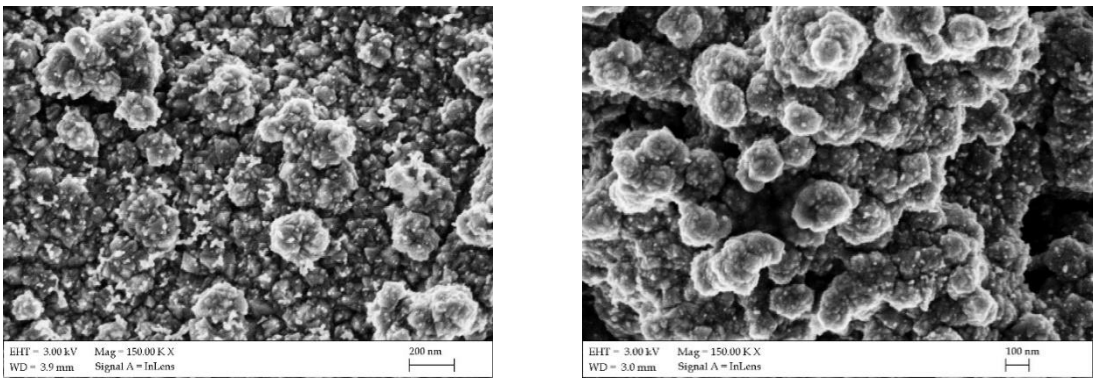

(**a**) (**b**)

Figure 7. SEM surface topography images of the platinum on the FTO/ceramic tile (a) and FTO/nickel foil (b).

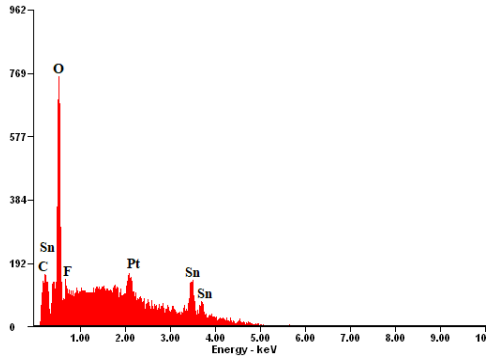

Figure 8. EDS spectrum of platinum on the FTO/ceramic tile substrate.

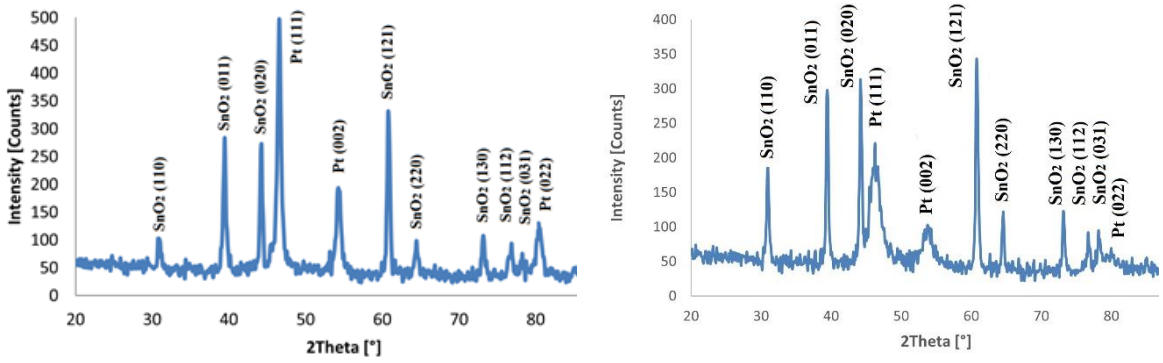

(**a**) (**b**)

Figure 9. The diffraction pattern of screen-printed platinum thin film deposited on the FTO/ceramic tile (a) and FTO/nickel foil (b).

In the Nyquist diagram of the layers used as the counter electrodes of dye-sensitized solar cells, two semicircles overlap each other in time due to their similar time constants (Figure 10). The platinum layers deposited on the FTO/ceramic tile and FTO/nickel foil have similar charge transfer resistance values of 27.3 and 26.5 Ω, respectively (Table 2).

Preprints (www.preprints.org) | NOT PEER-REVIEWED | Posted: 20 May 2021 doi:10.20944/preprints202105.0466.v1

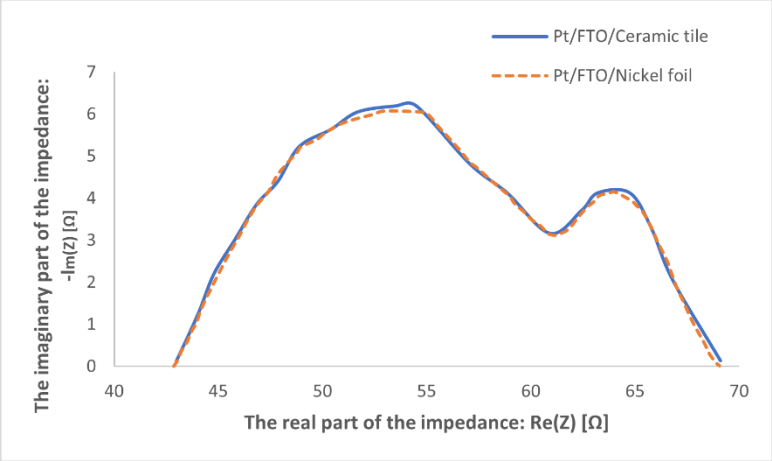

Figure 10. The EIS spectra of screen-printed platinum thin films deposited on the FTO/ceramic tile and FTO/nickel foil.

Table 2. Values of charge transfer resistance R_{ct} and solution resistance R_s from the EIS spectra of the produced counter electrodes.

Pt samples	***R_{ct} [Ω]***	***R_s [Ω]***
Nickel foil	26.5	42.5
Ceramic tile	27.3	41.8

Electrical parameters of manufactured DSSCs were characterized by measuring the current-voltage (I-V) characteristics using PV Test Solutions Tadeusz Zdanowicz Solar Cell I-V Tracer System and a Keithley 2400 source meter under standard AM 1.5 radiation. It can be seen that the shape of the current-voltage characteristic of the solar cell with a ceramic tile counter electrode was less rectangular than the solar cell with a glass counter electrode. It can be seen (Figure 11) that the nickel foil and tile substrates had a slight influence on the short-circuit current and open-circuit voltage, which consequently affected the efficiency of the dye-sensitized solar cells.

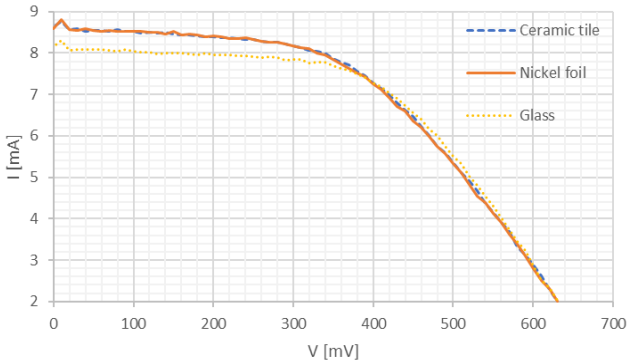

Figure 11. Current-voltage characteristics of experimental DSSCs.

The basic electrical parameters of the measured solar cells are presented in Table 3. Analysis of the measured electrical parameters showed that the cells with a ceramic tile had a higher efficiency than the cell with nickel foil from among the produced integrated solar cells.

 doi:10.20944/preprints202105.0466.v1

Table 3. Electrical parameters of experimental DSSCs.

DSSC sample	I_{sc} *[mA]*	V_{oc} *[mV]*	I_{max} *[mA]*	V_{max} *[mV]*	P_{max} *[mW]*	*FF*	E_{ff} *[%]*
Nickel foil	8.695	628.998	6.989	417.956	2.817	0.54	4.07
Ceramic tile	8.728	629.988	7.018	417.248	2.838	0.54	4.22
Glass	8.737	631.821	6.906	414.501	2.969	0.53	4.89

4. Conclusions

Building-integrated dye-sensitized solar cells were manufactured based on ceramic tile and nickel foil substrates. The advantage of this solution is a high level of integration with construction while requiring the same time to generate electricity. To produce a counter electrode, a layer of transparent conductive oxide in the form of fluorine-doped tin oxide (FTO) was deposited by an atomization method. The crystalline structure of atomized FTO was recorded. Then, a platinum paste was applied on the FTO tile and foil using a screen-printing method to construct a counter electrode. The SEM studies confirmed that a layer of FTO was deposited without major contamination or damage, and the grain size did not exceed 100 nm. The electrical properties of the dye-sensitized solar cells with a ceramic tile and foil as the counter electrode were the highest, which was close to the efficiency of a solar cell using conventional glass as the counter electrode. Such electrodes demonstrate the possibility of fabricating stable, low-cost, and effective building-integrated dye-sensitized solar cells.

Author Contributions: Conceptualization, MS (Marek Szindler); Methodology, MS (Marek Szindler), MS (Magdalena Szindler), AD, KL; Validation, M.S. (Marek Szindler), MS (Magdalena Szindler),; Formal analysis, MS (Marek Szindler), MS (Magdalena Szindler), AD, KL, PK; Investigation, MS (Marek Szindler), MS (Magdalena Szindler), AD, KL, PK, RP; Data duration, MS (Marek Szindler), MS (Magdalena Szindler); Writing—original draft preparation, MS (Marek Szindler); Writing—review and editing, MS (Marek Szindler),;Project administration, MS (Marek Szindler); Funding acquisition, MS (Marek Szindler),

All authors have read and agreed to the published version of the manuscript.

Funding: This publication was supported under the scholarship fund of the Silesian University of Technology in the field of scientific research and development works, Year 2020.

Acknowledgments: This publication was supported under the scholarship fund of the Silesian University of Technology in the field of scientific research and development works, Year 2020.

Conflicts of Interest: The authors declare no conflict of interest.

 doi:10.20944/preprints202105.0466.v1

References

1. Battaglia, C.; Cuevas, A.; De Wolf, S. High-efficiency crystalline silicon solar cells: Status and perspectives. *Energy Environ. Sci*. **2016**, *9*, 1552–1576.
2. Masuko, K.; Shigematsu, M.; Hashiguchi, T.; Fujishima, D.; Kai, M.; Yoshimura, N.; Yamaguchi, T.; Ichihashi, Y.; Mishima, T.; Matsubara, M.; et al. Achievement of More than 25% Conversion Efficiency with Crystalline Silicon Heterojunction Solar Cell. *IEEE J. Photovolt*. **2014**, *4*, 1433–1435.
3. Deng, S.; Wang, R.Z.; Dai, Y.J. How to evaluate performance of net zero energy building—A literature research. *Energy* **2014**, *71*, 1–16.
4. De Santoli, L. Guidelines on energy efficiency of cultural heritage. *Energy Build*. **2015**, *86*, 534–540. Heinstein, P.; Ballif, C.; Perret-Aebi, L.-E.E. Building integrated photovoltaics (BIPV): Review, potentials, barriers and myths. *Green* **2013**, *3*, 125–156.
5. Jelle, B.P.; Breivik, C.; Røkenes, H.D. Building integrated photovoltaic products: A state-of-the-art review and future research opportunities. *Solar Energy Mater. Solar Cells* **2012**, *100*, 69–96.
6. Yen-Chieh Huang et al. Development of building integrated photovoltaic (BIPV) system with PV ceramic tile and its application for building façade. *Energy Procedia* **2014**, *61*, 1874–1878.
7. Debbarma M. et al. Comparison of BIPV and BIPVT: A review. *Resource-Efficient Technologies*, **2017**, *3*, 263–271.
8. O'Regan, B.; Grätzel, M. A low-cost, high-efficiency solar cell based on dye-sensitized colloidal TiO2 films. *Nature* **1991**, *353*, 737–740
9. Ferber, J.; Stangl, R.; Luther, J. An electrical model of the dye-sensitized solar cell. *Sol. Energy Mater. Sol. Cells* **1998**, *53*, 29–54.
10. Liang, M.; Chen, J. Arylamine organic dyes for dye-sensitized solar cells. *Chem. Soc. Rev. 2013*, **42**, 3453.
11. Ezhov, A.V.; Zhdanova, K.A.; Bragina, N.A.; Mironov, A.F. Approaches to Improve Efficiency of Dye-Sensitized Solar Cells. Macroheterocycles 2016, 9, 337–352.
12. Yang, J.; Ganesan, P.; Teuscher, J.; Moehl, T.; Kim, Y.J.; Yi, C.; Comte, P.; Pei, K.; Holcombe, T.W.; Nazeeruddin, M.K.; et al. Influence of the Donor Size in D−π–A Organic Dyes for Dye-Sensitized Solar Cells. *J. Am. Chem. Soc*. **2014**, *136*, 5722–5730.
13. Li, Y.; Li, Y.; Song, P.; Ma, F.; Liang, J.; Sun, M. Screening and design of high-performance indoline-based dyes for DSSCs. *RSC Adv*. **2017**, *7*, 20520–20536.
14. Bella, F.; Galliano, S.; Gerbaldi, C.; Viscardi, G. Cobalt-based electrolyte for dye-sensitized solar cells: Recent advances towards stable devices. *Energies* **2016**, *9*, 384.
15. Raj, A.C.; Prasanth, R. A critical review of recent developments in nanomaterials for photoelectrodes in dye-sensitized solar cells. J. Power Sources ***2016,*** 317, 120–132.
16. Gerosa, M.; Sacco, A.; Scalia, A.; Bella, F.; Chiodoni, A.; Quaglio, M.; Tresso, E.; Bianco, S. Toward totally flexible dye-sensitized solar cells based on titanium grids and polymeric electrolyte. *IEEE J. Photovolt*. **2016**, *6*, 498–505.
17. Milan, R.; Selopal, G.S.; Epifani, M.; Natile, M.M.; Sberveglieri, G.; Vomiero, A.; Concina, I. ZnO/SnO2 engineered composite photoanodes for dye-sensitized solar cells. *Sci. Rep*. **2015**, *5*, 14523.
18. Clifford, J.N.; Palomares, E.; Nazeeruddin, M.K.; Grätzel, M.; Nelson, J.; Li, X.; Long, N.J.; Durrant, J.R. Molecular control of recombination dynamics in dye-sensitized nanocrystalline TiO2 films: Free energy vs. distance dependence. *J. Am. Chem. Soc.* **2004**, *126*, 5225–5233.
19. Shimada K. et al. Platinum counter electrodes for dye-sensitized solar cells prepared by one-step dipping process Jpn. *J. Appl. Phys.* **2019**, 58, 1–4.
20. Yu-Hsun N. et al. Study of How Photoelectrodes Modified by TiO2/Ag Nanofibers in Various Structures Enhance the Efficiency of Dye-Sensitized Solar Cells under Low Illumination, Energies **2020**, 13, 1–14